

EXPERIMENTAL CHARACTERIZATION OF MICRO VORTEX GENERATORS IN LOW-SPEED FLOWS

M. Tuğrul Akpolat¹
Roketsan Missiles Inc.
Ankara, Turkey

Anas Abdulrahim², Abdelrahman Hassanein³, Oğuz Uzol⁴,
Mustafa Perçin⁵
METU Center for Wind Energy Research (RÜZGEM)
Ankara, Turkey

ABSTRACT

In this study, we present the experimental results of the characterization of micro-ramp type Micro Vortex Generators (MVGs) in low-speed flows. The undisturbed boundary layer profile was measured by means of Hot-Wire Anemometry. Two MVGs with the same design but different height-to-boundary layer thickness ratios are used in this study. Two-dimensional two-component particle image velocimetry measurements are conducted in the wake of the MVGs. The results reveal the lift-off of the wake away from the wall further downstream, which is an indication of the streamwise counter-rotating vortex pair induced by the MVGs. In addition, it was observed that with the MVG having a larger height-to-boundary layer thickness ratio, a wake having a higher wall-normal velocity distribution with a slower upwash motion recovery is induced. This is attributed to the stronger counter-rotating vortex pair produced by the larger MVG. Finally, a wake scaling procedure is applied in order to assess the self-similarity of the wake velocity profiles.

NOMENCLATURE

2D2C	Two-dimensional two-component
c	Chord
H	Shape factor
HWA	Hot-Wire Anemometry
MVG	Micro Vortex Generator
PIV	Particle Image Velocimetry
Re_θ	Reynolds number based on momentum thickness
U	Streamwise velocity
\bar{U}	Normalized streamwise velocity

¹ Lead Engineer, Propulsion Systems Design Department. PhD Candidate, Department of Aerospace Eng., Middle East Technical University (METU) Email: tugrul.akpolat@roketsan.com.tr

² Scientific Project Expert, RÜZGEM. PhD Candidate, Department of Aerospace Eng., METU Email: aanas@metu.edu.tr

³ Graduate Student, Department of Aerospace Eng., METU Email: e224628@metu.edu.tr

⁴ Prof. Dr., Department of Aerospace Eng., METU. Head, RÜZGEM. Email: uzol@metu.edu.tr

⁵ Asst. Prof. Dr., Department of Aerospace Eng., METU. Coordinator, RÜZGEM Exp. Aerodynamics Lab. Email: mpercin@metu.edu.tr

U^+	Dimensionless velocity
U_∞	Freestream velocity
U_{BL}	Velocity in the undisturbed boundary layer
U_{eff}	Effective velocity
$U\tau$	Friction velocity
V	Wall-normal velocity
V_{max}	Maximum value of upwash velocity
w	Width
\bar{y}	Normalized y-coordinate
y^+	Dimensionless y-coordinate
α	MVG half-angle
δ	Boundary layer thickness
δ^*	Displacement thickness
$\Delta U_{deficit}$	Streamwise velocity deficit
θ	Momentum thickness
Ω_z	Out-of-plane vorticity

INTRODUCTION

Micro Vortex Generators (MVGs), also known as low-profile vortex generators or sub-boundary layer vortex generators, have a height of 10%-50% of the boundary layer thickness. MVGs, affect the boundary layer by generating a counter-rotating vortex pair in the streamwise direction, consequently promoting mixing between the low-momentum near-wall region and the relatively-high-momentum upper region of the boundary layer (Figure 1). The endorsed momentum transfer between the upper and the lower (near-wall) regions of the boundary layer results in a more energized boundary layer which is less prone to boundary layer separations [Lin, 2002].

Vortex generators are a passive means of flow control, i.e., they cannot be moved, altered, or removed in the off-design conditions which results in addition of excess drag to the system. As conventional vortex generators do, MVGs also promote momentum exchange between the low and high momentum regions in the boundary layer by generating vorticity in the streamwise direction. However, the difference between a conventional vortex generator and an MVG is that the former promotes the mixing between the boundary layer and the freestream flow, whereas the latter does that inside the boundary layer itself. Being restrained inside the boundary layer, MVGs are small by their nature, resulting in a reduced drag in both on and off-design conditions. MVGs have a wide range of applications such as aircraft noise reduction [Holmes *et al.* 1987], enhancing engine inlet performance [Babinsky *et al.*, 2007], flow separation control on wings, wing extensions and wind turbines [Bohannon, 2006; Skrzypiński *et al.*, 2014]. In wind turbines, vortex generators are generally used below about 30% span to reduce the effects of flow separation in this region. They are also used near the blade tip region to increase blade performance by delaying stall under leading edge erosion or contamination conditions [Skrzypiński *et al.*, 2014]. Additional drag due to VGs is a critical issue in wind turbines and needs to be minimized to prevent reduction in Annual Energy Production levels [Fernandez-Gamiz *et al.*, 2017; Velte & Hansen, 2013].

In this respect, the main objective of this study is to characterize ramp type MVGs, i.e., micro-ramps, for low-speed applications. The undisturbed boundary layer was obtained via hot-wire anemometry (HWA) measurements., Two-dimensional two-component particle image velocimetry (2D2C PIV) measurements are performed in the wake of the MVGs in order to observe the wake characteristics in low-speed flows. In addition, a wake scaling analysis was employed on the wake velocity profiles.

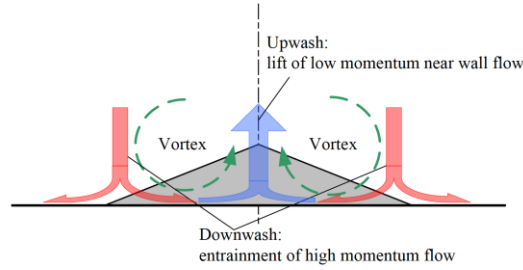


Figure 1: Rear view of a micro-ramp with the counter-rotating vortices, upwash and downwash motions are marked [Sun 2014].

METHODOLOGY

Wind Tunnel Facility

The experimental work is done in the METUWIND C3 open-return suction type boundary layer wind tunnel (Figure 2) located at METU Center for Wind Energy (RÜZGEM). The test section of the wind tunnel is 1 x 1 x 8 m³ (height x width x length), allowing for measurements with relatively large boundary layer thickness values. The maximum velocity is 25 m/s with a turbulence intensity of about 0.35%.



Figure 2: The METUWIND C3 Wind Tunnel.

Undisturbed Boundary Layer Measurements

The undisturbed boundary layer measurements are performed at the Reynolds number of 4836 based on the momentum thickness and freestream velocity ($U_\infty = 10.1$ m/s). Figure 3 shows a general sketch of the setup and relevant coordinate system used as a reference for the measurements. The MVG is located 6.27 m downstream of the inlet of the test section. HWA measurements are conducted 6.20 m downstream of the test section inlet as shown in Figure 3. The HWA measurements were conducted without the presence of any MVGs. The boundary layer is measured by traversing a single sensor boundary layer hot-wire probe in the wall normal direction (y-axis) spanning a distance of 210 mm, with step sizes of 1 mm up to 100 mm distance and 2 mm up to 210 mm distance. Velocity data is collected at a sampling rate of 10 kHz for a duration of 30 seconds at each measurement point.

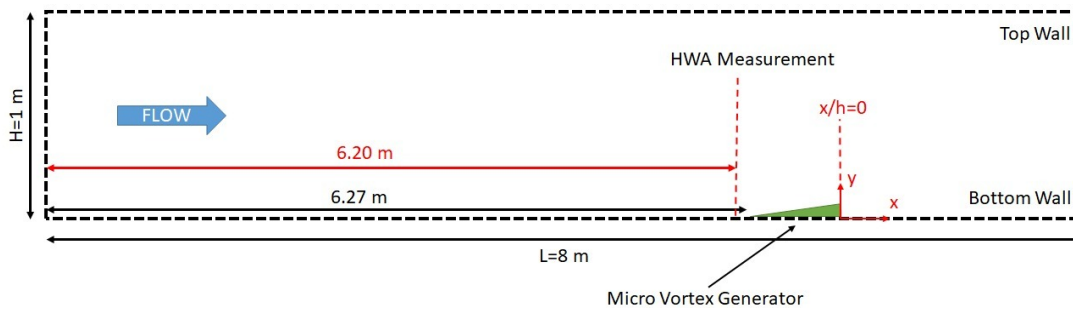


Figure 3: Schematic layout of the wind tunnel test section and MVG measurement setup.

Figure 4 shows the variation of the streamwise velocity (U , x-component of velocity) normalized with the freestream velocity (U_∞) and the streamwise turbulence intensity profiles for the undisturbed boundary layer. The boundary layer thickness is estimated to be 111.3 mm from the bottom wall (by using the velocity gradient profile in the wall-normal direction after applying a running-average filter to the velocity profile with a kernel size of 9 data points). Based on this boundary layer thickness, other boundary layer parameters such as the displacement thickness, the momentum thickness and the shape factor are calculated and presented in Table 1.

Figure 5 shows the dimensionless velocity U^+ ($U^+ = U/U_\tau$) and the length scale y^+ ($y^+ = yU_\tau/\nu$) normalized with the friction velocity. The friction velocity ($U_\tau = \sqrt{\tau/\rho}$) is estimated from the wall shear stress (τ). The wall shear stress was estimated from the velocity gradient ($\tau = \mu dU/dy$). It can be seen that the region of $y^+ = 350$ to 2500 is resolved by means of the HWA measurements.

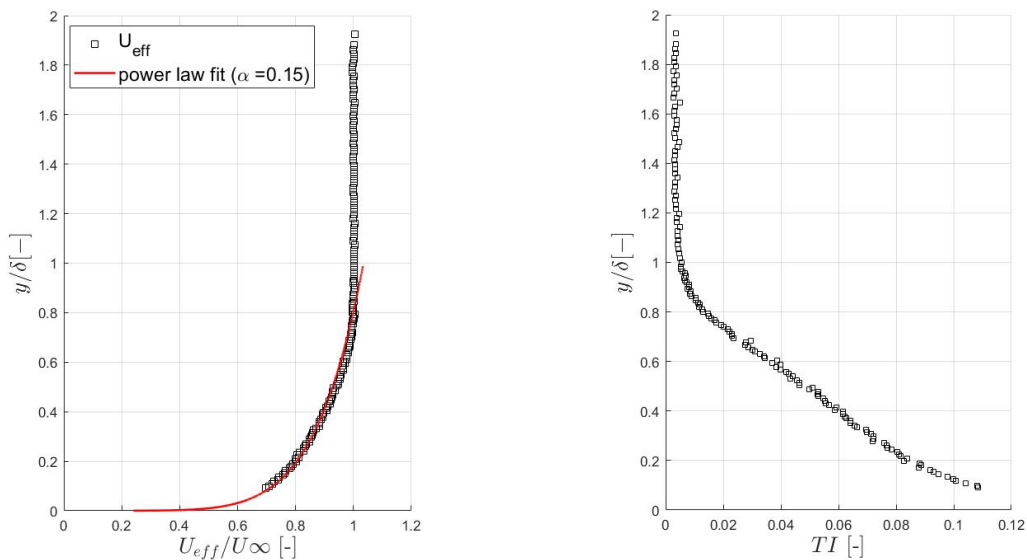


Figure 4: Vertical velocity and turbulence intensity profiles of the incoming flow.

Table 1: Undisturbed Boundary Layer Properties.

α	$\bar{\delta}$ (mm)	$\bar{\delta}^*$ (mm)	θ (mm)	H	Re_θ	U_τ (m/s)
0.15	111.31	8.11	6.74	1.2	4836	0.2614

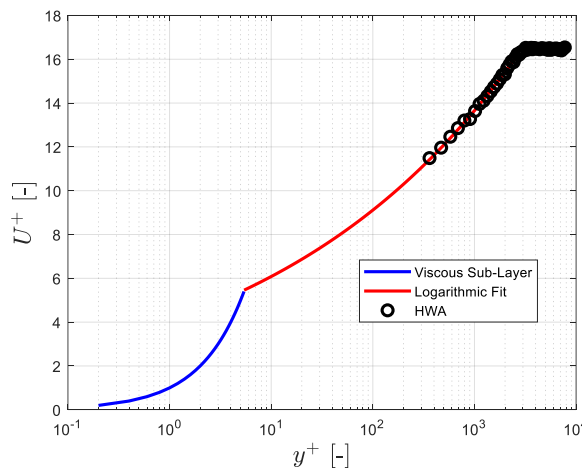


Figure 5: Law of the wall. Dimensionless streamwise velocity of the undisturbed boundary layer.

Design of the Micro Vortex Generator

The ramp-type MVGs used in this study have the same design as those which were used by Sun [Sun, 2014]. The design parameters are given in the sketch shown in Figure 6. Both MVGs were produced by employing a 3D printer. The solid models of the MVGs and the produced models are shown in Figure 6. The dimensions of the MVGs are given in Table 2 along with the corresponding h/δ ratios.

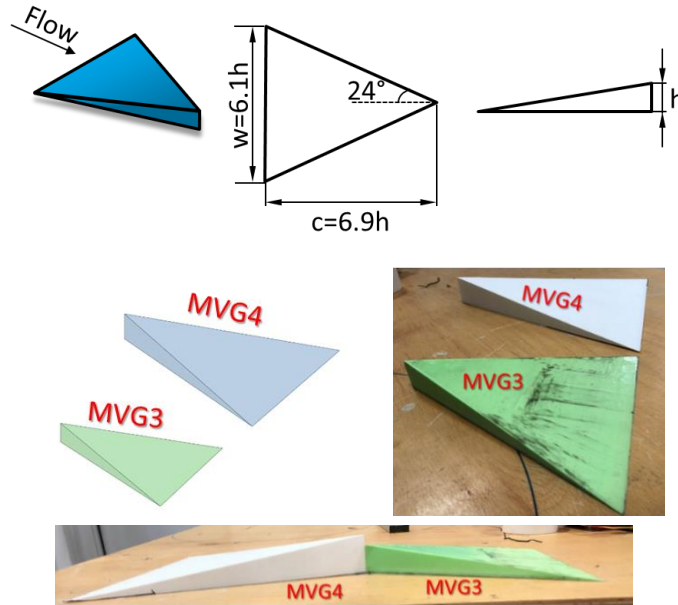


Figure 6: The design of the micro vortex generator.

Table 2: MVG dimensions with h/δ ratios.

MVG	h	w	c	α	h/δ
Design	-	6.1h	6.9h	24°	-
MVG3	30 mm	183 mm	207 mm	24°	0.27
MVG4	40 mm	244 mm	276 mm	24°	0.36

Wake Measurements

Two-Dimensional Two-Component Particle Image Velocimetry (2D2C PIV)

2D2C PIV measurements are conducted downstream of the Micro Vortex Generators (MVG) in a streamwise-oriented plane that is aligned with the central axis of the MVG. The PIV setup consists of a New Wave Research Solo 120XT Nd:YAG 532 nm laser, a camera with CMOS sensor, optics and a 3D heavy-duty traverse system as shown in Figure 7.

The flow is seeded with fog of droplets with a mean diameter of $1 \mu\text{m}$. Double-frame particle images are preprocessed by applying opening, closing and median filters in order to improve the image quality and remove any background noise. Image masking was applied in order to mask out the MVGs since they are located in the camera field of view. Then, using a two-step adaptive correlation analysis with the final interrogation window of 32×16 pixels² and 50% overlap, a vector spacing of 1.2 mm along the streamwise direction and 0.6 mm along the wall-normal direction is obtained in the resulting vector maps. The time between the two laser pulses is defined as $70 \mu\text{s}$ and the repetition rate is selected to be 10 Hz. The whole system, including the camera, laser and the optics is traversed in the streamwise (x) and wall-normal (y) directions. The final field of view for MVG3 is $x/h=0.5$ to 23; $y/h=0$ to 7.5, whereas field of view for MVG4 is $x/h=0.5$ to 16; $y/h=0$ to 5.5. This was achieved by taking data in 8 different windows by traversing in the streamwise direction and in the wall-normal direction.

Measurement domains for both MVGs are shown in Figure 8. 1000 image pairs were taken in all 8 measurement windows, and the resultant vector fields are stitched to provide a clear picture of the flow pattern in the wake of the MVGs.

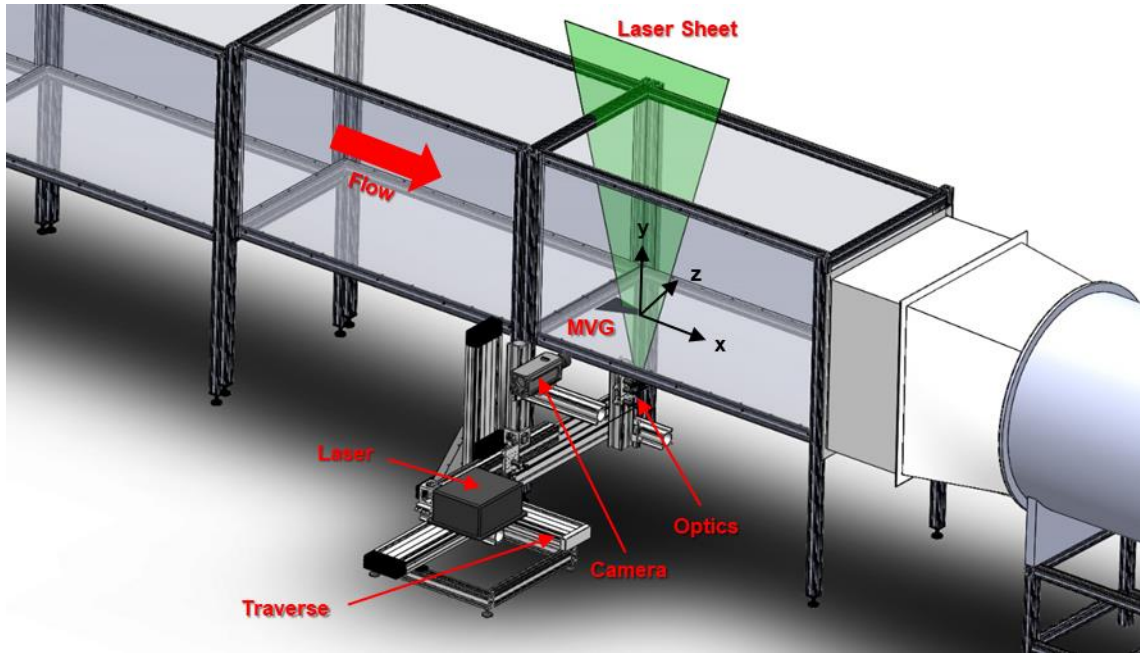


Figure 7. PIV measurement setup for micro vortex generator (MVG) wake measurements

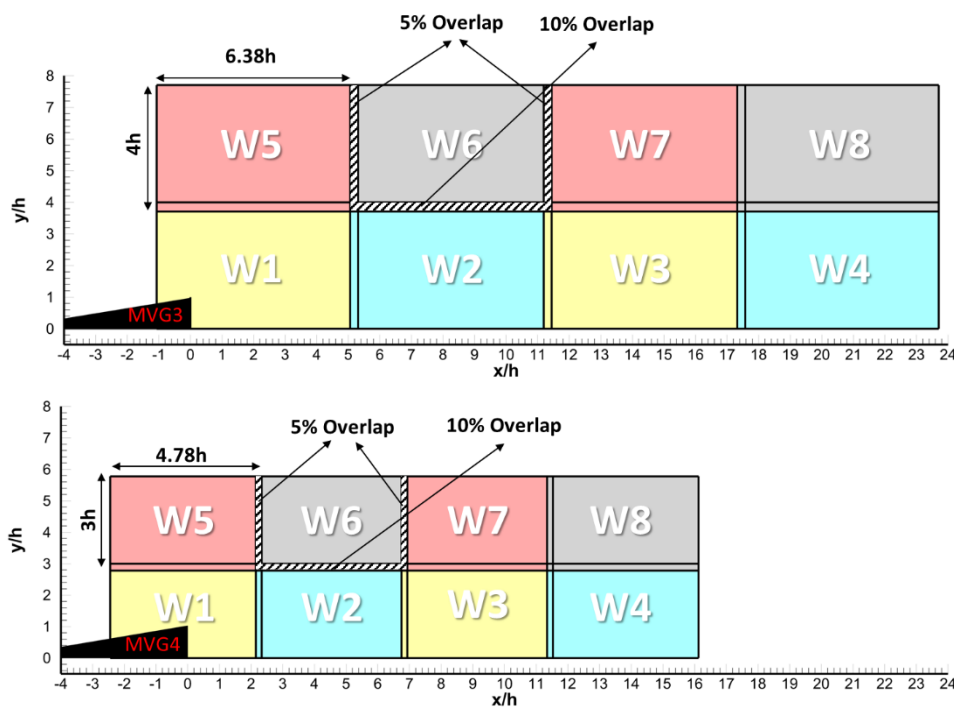


Figure 8: PIV measurement domain showing the windows with the overlap regions and the field of view dimensions.

Results

Mean wake flow field

Figure 9 shows the contours of streamwise velocity normalized by the freestream velocity for MVG3 (top panel) and MVG4 (bottom panel). It is seen that the wakes produced by both MVGs are similar. Results clearly demonstrate the lift-off the MVG wake further downstream. The lift-off is characterized by the movement of the maximum velocity deficit away from the wall. It is evident from the streamwise velocity contours that the MVG4 causes slightly higher lift-off comparing to that of the MVG3. This is also an indication of the upwash motion created by the streamwise counter-rotating vortex pair generated by the MVGs which can also be seen in the wall-normal velocity contours (Figure 10). In Figure 10, it is clear that the upwash motion created by the MVG4 is stronger, as it is expected to create a stronger counter-rotating vortex pair compared to MVG3. This is also evident in the out-of-plane vorticity contours (Figure 11). The out-of-plane vorticity distribution also shows that the vorticity is increased in the near wall region by both MVGs.

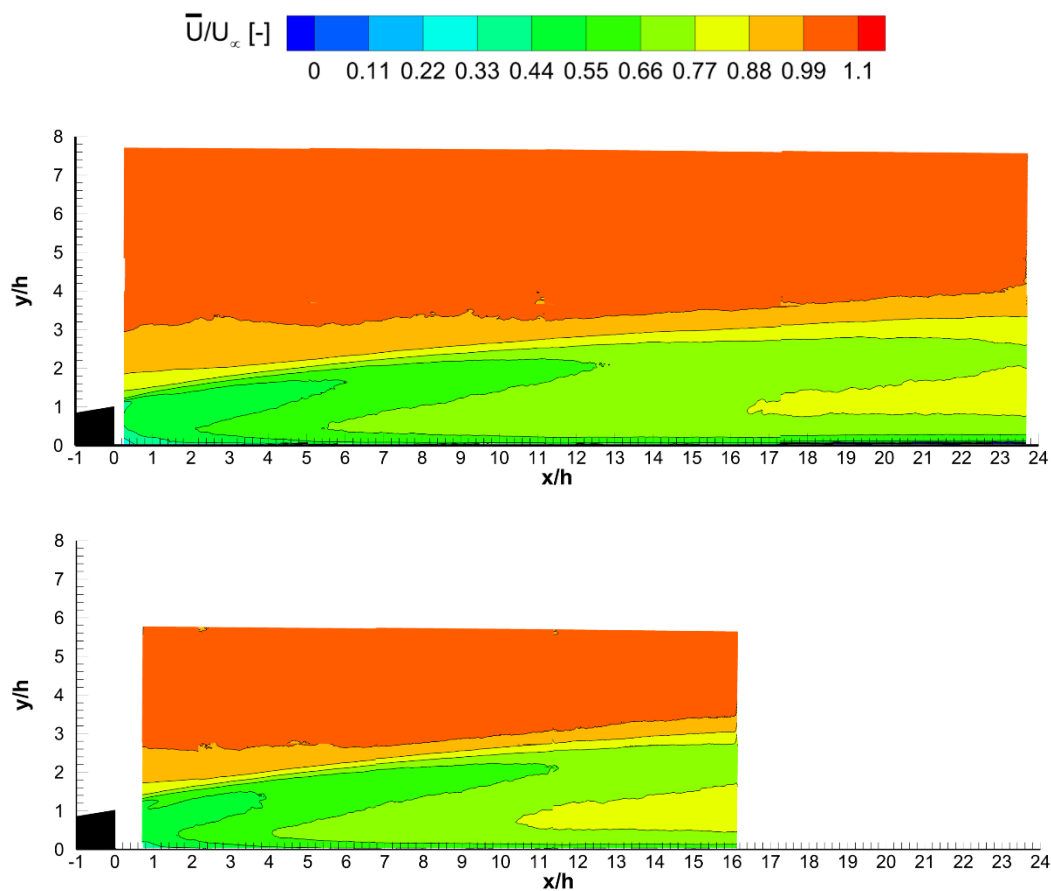


Figure 9: Contours of normalized streamwise velocity; top: MVG3, bottom: MVG4.

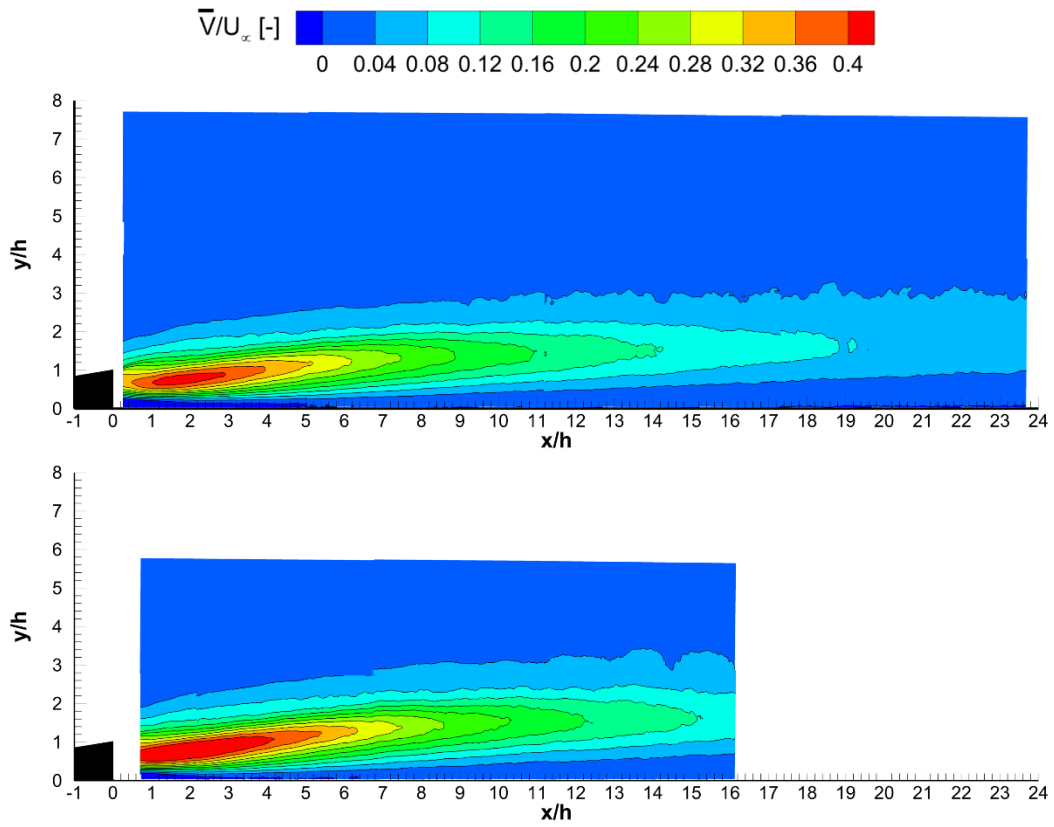


Figure 10: Contours of normalized wall-normal velocity; top: MVG3, bottom: MVG4.

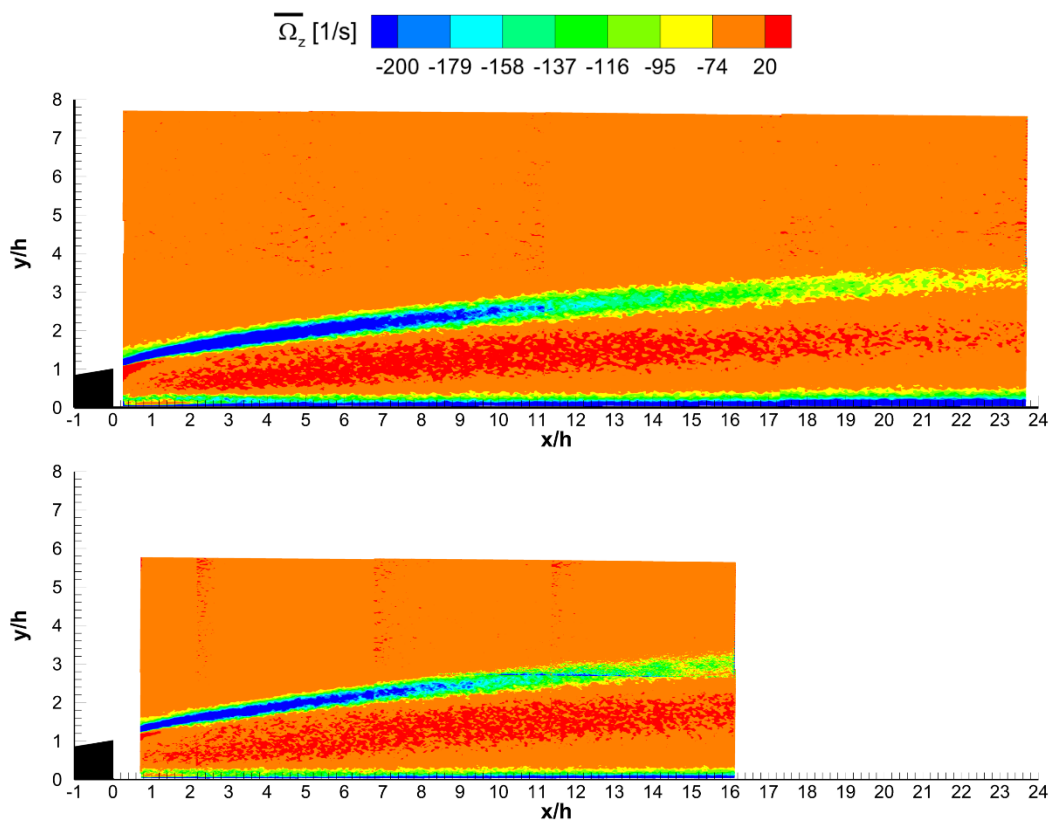


Figure 11: Contours of out-of-plane vorticity field; top: MVG3, bottom: MVG4.

Comparisons of wake velocity profiles

The wake velocity profiles are extracted from the 2D2C PIV data, for both streamwise and wall-normal velocities. Figure 12 shows the development of the wake normalized streamwise velocity profiles in the streamwise direction. One could observe the location of the minimum velocity (*i.e.* maximum velocity deficit) shifts upwards further downstream for both MVGs. This is due to the upwash motion in the wake created by the counter-rotating vortices which are induced by the MVGs. Figure 13 shows the development of the normalized wall-normal velocity profiles in the streamwise direction. The recovery of the upwash motion created by the MVG3 is much faster than that created by MVG4.

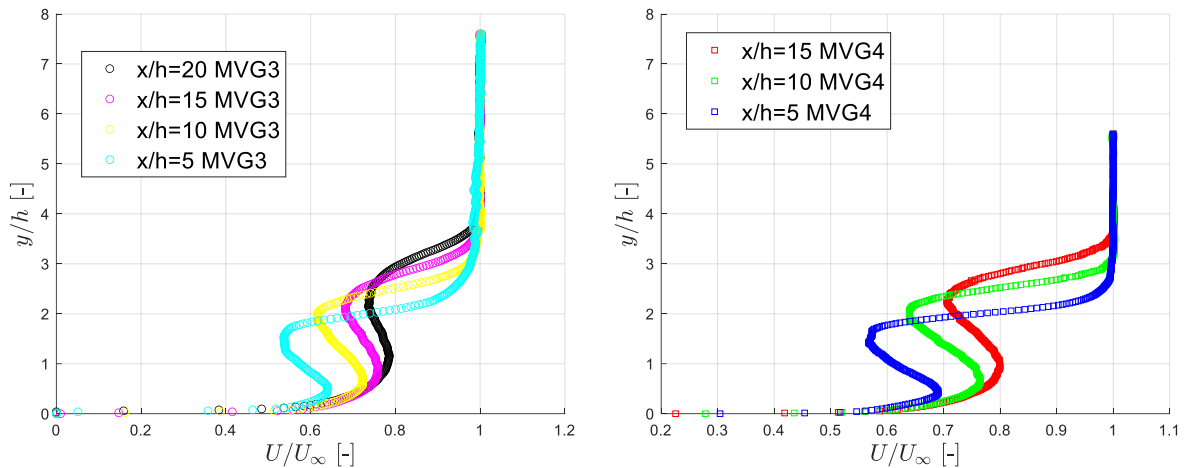


Figure 12: Normalized streamwise velocity at different streamwise positions downstream of the MVG. MVG3 (left) and MVG4 (right).

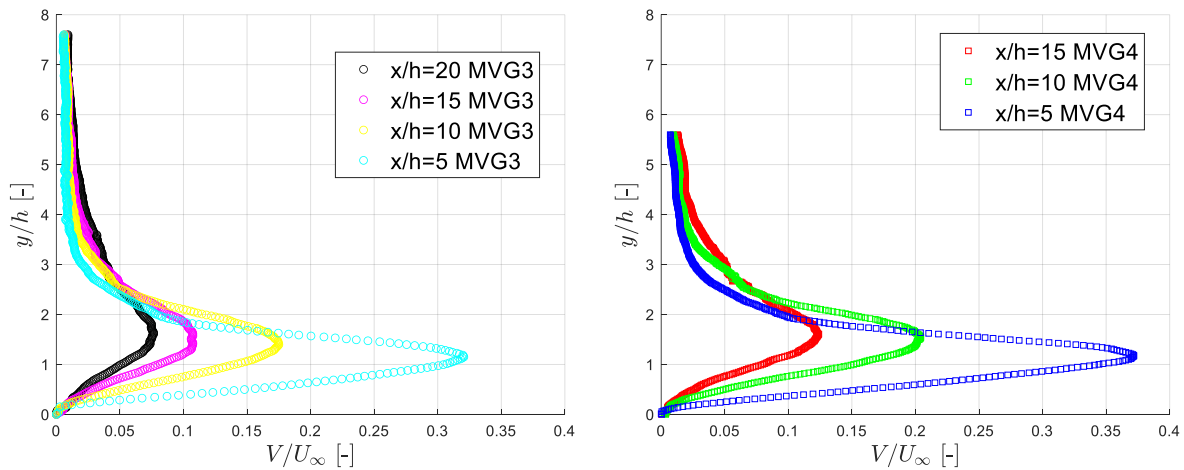


Figure 13: Normalized wall-normal velocity at different streamwise positions downstream of the MVG. MVG3 (left) and MVG4 (right).

Figure 14 shows the wake velocity profile for normalized streamwise velocity for both MVGs at $x/h=5, 10$ and 15 . It can be seen that the streamwise velocity profiles of the MVG3 and the MVG4 are quite similar, with a slight difference. The maximum velocity deficit shown in the streamwise velocity profiles (at $x/h=5$) is 54% for the MVG3 whereas it is 57% for the MVG4. The profiles for normalized wall-normal velocity (Figure 15) also demonstrates that similar wakes are created by the two MVGs. However, in the case of normalized wall-normal velocity profiles the difference between the two MVGs is more pronounced, especially in the near wake region. As can be seen from the profiles of the wall-normal velocity, velocities induced by MVG4 are higher compared to that induced by MVG3, this is seen especially in the upper part of the wake.

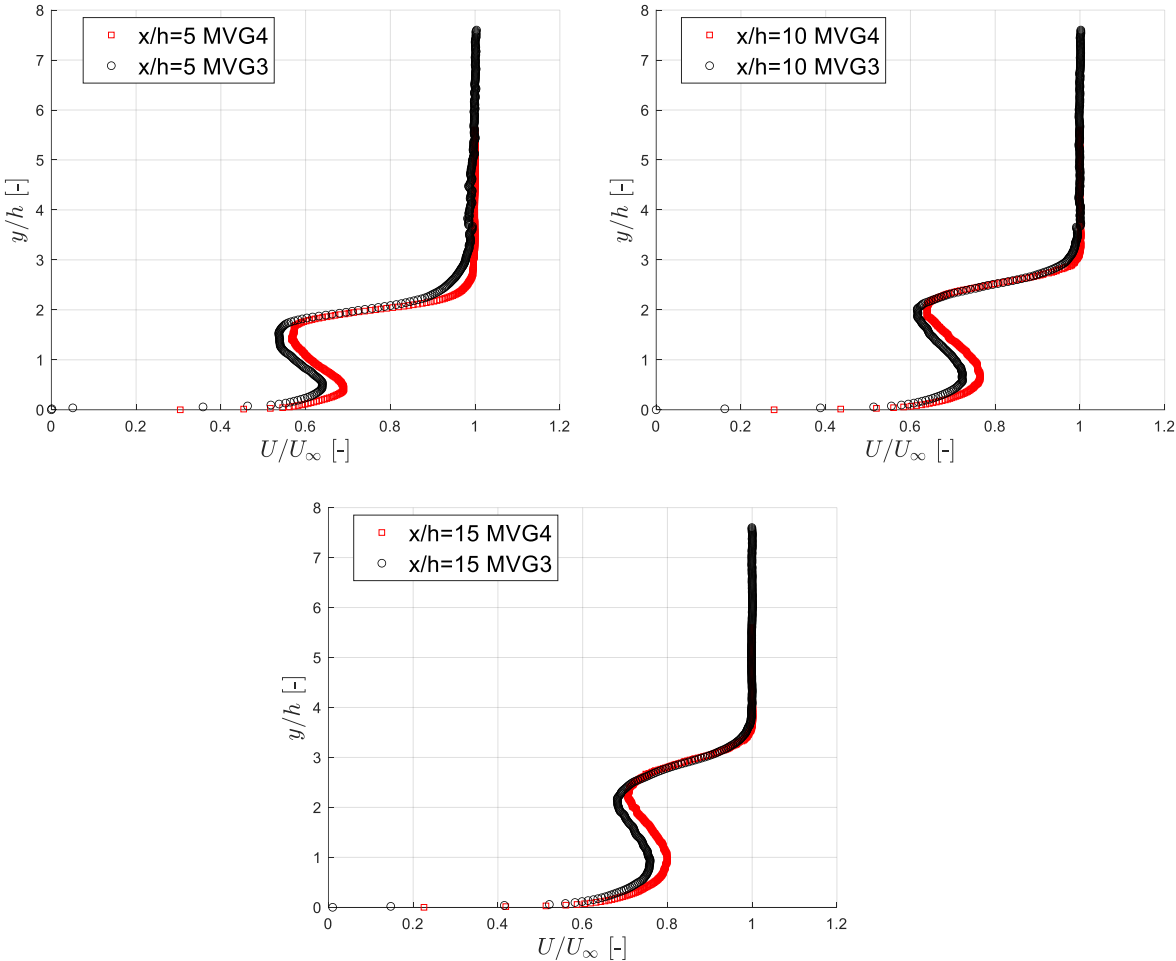


Figure 14: Comparison of normalized streamwise velocity between MVG3 and MVG4 at different downstream positions.

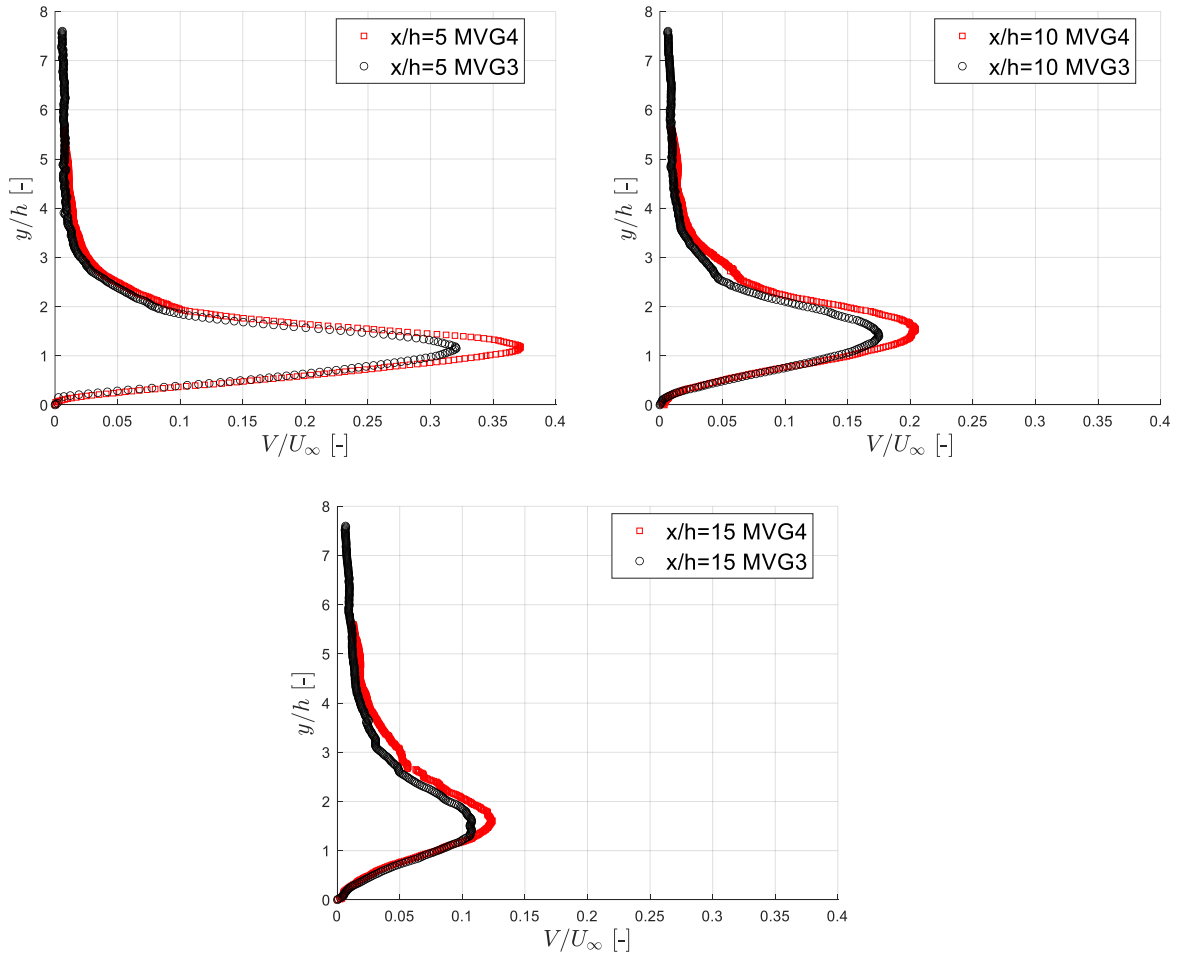


Figure 15: Comparison of normalized wall-normal velocity between MVG3 and MVG4 at different downstream positions.

Self-similarity of wake velocity profiles

Streamwise and wall-normal components of velocity are scaled in order to find out if the wake is self-similar using the methodology employed by [Sun, 2014] for the wake scaling. The streamwise component is scaled in order to have a distribution with maximum deficit having the value of $\bar{U}_{deficit} = -1$. The wall-normal velocity is scaled with the maximum upwash velocity (V_{max}), with the aim of having a scaled maximum upwash velocity of $V_{max} = 1$. Figure 16 shows a sketch that summarizes the parameters used in the scaling process of the velocity components.

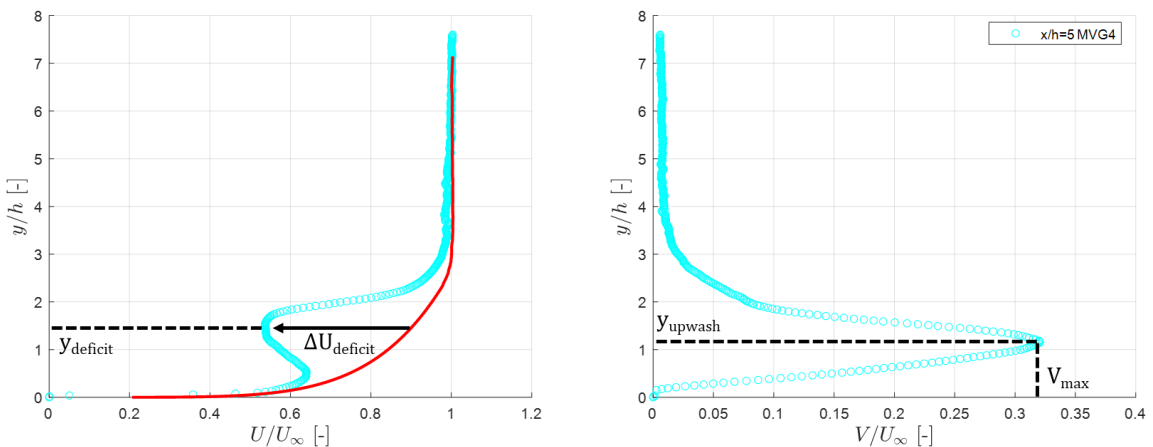


Figure 16: Visualization of the parameters used in the wake scaling equations.

The streamwise velocity is scaled by using below equation.

$$\bar{U}(y) = \frac{U(y) - U_{BL}(y)}{\Delta U_{deficit}}$$

Where, $U(y)$ is the velocity at the wake, $U_{BL}(y)$ is the velocity extracted from the undisturbed boundary layer, and $\Delta U_{deficit}$ is the velocity difference between the undisturbed boundary layer and the wake velocity at the same y position.

The y -coordinate is scaled by taking the difference with the position of the maximum deficit ($y_{deficit}$) as shown in Figure 16.

$$\bar{y} = \frac{y - y_{deficit}}{y_{deficit}}$$

In addition, the wall-normal velocity is scaled by the maximum upwash velocity (V_{max}).

$$\bar{V}(y) = \frac{V(y)}{V_{max}}$$

For the wall-normal velocity, the y -coordinate is scaled by using the equation below.

$$\bar{y} = \frac{y - y_{upwash}}{y_{upwash}}$$

Where, y_{upwash} is the position of the maximum upwash velocity.

Figure 17 shows the scaled wake velocity profiles of the streamwise (left) and wall-normal (right) velocity components at different downstream positions (x/h) for the two MVGs. As one could observe, the streamwise velocity profiles collapse into a single distribution except at $x/h=5$ at the lower half of the wake. On the other hand, the wall-normal velocity shows a good collapse on the lower part of the wake, whereas the upper half of the wake shows a discrepancy above $\bar{y} = 0.5$. This is most probably due to the wall-normal velocity magnitude being reduced towards the freestream flow.

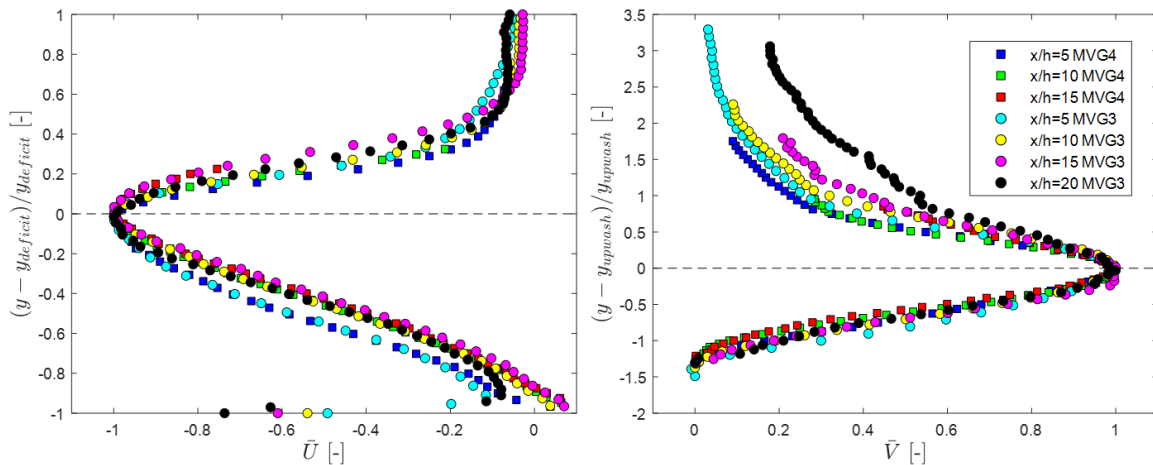


Figure 17: Self-similarity of the velocity profiles. Streamwise velocity (left) and wall-normal velocity (right). Legend is the same for both figures.

Conclusions

Results of an experimental study, with the aim to investigate the wake characteristics produced by MVGs are presented in low-speed flows. For the sake of the MVG height classification (h/δ), boundary layer properties measured via hot-wire anemometry, yielding a boundary layer thickness of 111.3 mm at a freestream velocity of 10.1 m/s. The wake properties of two MVGs having the same design parameters but different heights (30 mm and 40 mm, corresponding to MVG3 and MVG4 respectively) were measured via two-dimensional two-component particle image velocimetry. The results clearly demonstrate the upwash motion created by the counter-rotating vortex pair which is induced by the MVGs. It is clear that MVG4 induces a higher wall-normal velocity as a consequence of stronger counter-rotating vortex pair promoted by the larger MVG. As the normalized wall-normal wake velocity profiles demonstrate, it is obvious that the recovery of the upwash motion created by MVG3 is much faster than that created by MVG4. Scaling of the wake velocity profiles for streamwise and wall-normal velocity was also implemented in order to assess self-similarity of the wake induced by the two MVGs. It is observed that the streamwise velocity profiles collapse into a single distribution except in the near wake region, whereas the self-similarity of the wall-normal velocity shows a good collapse on the lower part of the wake.

References

- Babinsky, H., Makinson, N. J., Morgan, C. E., (2007) *Micro-Vortex Generator Flow Control for Supersonic Engine Inlets*, 45th AIAA Aerospace Sciences Meeting and Exhibit, 8-11 January, Reno, Nevada, USA.
- Bohannon, K. S., (2006) *Passive Flow Control on Civil Aircraft Flaps using Sub-Boundary Layer Vortex Generators in the AWIATOR Programme*, 3rd AIAA Flow Control Conference, 5-8 June, San Francisco, California, USA.
- Fernandez-Gamiz U., Zulueta, E., Boyano, A., Ansoategui, I., Uriarte, I. (2017) *Five Megawatt Turbine Power Output Improvements by Passive Flow Control Devices*, *Energies*, 10, 742.
- Holmes, A. E., Hickey, P. K., Murphy, W. R., Hilton, D. A., (1987) *The Application of Sub-Boundary Layer Vortex Generators to Reduce Canopy "Mach Rumble" Interior Noise On the Gulfstream III*, AIAA 25th Aerospace Sciences Meeting, January 12-15, Reno, Nevada, USA.
- Lin, J. C., (2002) *Review of research on low-profile vortex generators to control boundary layer separation*, *Progress in Aerospace Sciences*, 38:389-420.
- Velte, C. M., Hansen, M. O. L., (2013) *Investigation of flow behind vortex generators by stereo particle image velocimetry on a thick airfoil near stall*, *Wind Energy*, 2013; 16:775-785.
- Sun, Z., (2014) *Micro Ramps in Supersonic Turbulent Boundary Layers An Experimental And Numerical Study*, Ph.D Thesis Dissertation, TU Delft.
- Skrzypiński W., Gaunaa, M., Bak C. (2014) *The Effect of Mounting Vortex Generators on the DTU 10MW Reference Wind Turbine Blade*, *J. Phys. Conf. Ser.* 524 012034.